New Journal of Physics
The open access journal at the forefront of physics

Deutsche Physikalische Gesellschaft DPG
IOP Institute of Physics

Published in partnership with: Deutsche Physikalische Gesellschaft and the Institute of Physics

OPEN ACCESS

RECEIVED
10 December 2014

REVISED
4 February 2015

ACCEPTED FOR PUBLICATION
10 February 2015

PUBLISHED
12 March 2015

PAPER

Optimization of plasma mirror reflectivity and optical quality using double laser pulses

G G Scott[1,2], V Bagnoud[3], C Brabetz[3], R J Clarke[1], J S Green[1], R I Heathcote[1], H W Powell[2], B Zielbauer[3], T D Arber[4], P McKenna[2] and D Neely[1,2]

[1] Central Laser Facility, STFC Rutherford Appleton Laboratory, Didcot OX11 0QX, UK
[2] Department of Physics SUPA, University of Strathclyde, Glasgow G4 0NG, UK
[3] PHELIX group, GSI Helmholtzzentrum für Schwerionenforschung GmbH, D-64291 Darmstadt, Germany
[4] Department of Physics, University of Warwick, Coventry CV4 7AL, UK

E-mail: graeme.scott@stfc.ac.uk

Keywords: plasma mirror, plasma reflectivity, double pulse, plasma optics, optical quality, laser plasma interaction

Abstract

We measure a record 96 ±2.5% specularly reflected energy fraction from an interaction with a plasma mirror (PM) surface preionized by a controlled prepulse and find that the optical quality is dependent on the inter pulse time delay. Simulations show that the main pulse reflected energy is a strong function of plasma density scale length, which increases with the time delay and reaches a peak reflectivity for a scale length of 0.3 μm, which is achieved here for a pulse separation time of 3 ps. It is found that the incident laser quasi near field intensity distribution leads to nonuniformities in this plasma expansion and consequent critical surface position distribution. The PM optical quality is found to be governed by the resultant perturbations in the critical surface position, which become larger with inter pulse time delay.

1. Introduction

In the chirped pulse amplification technique, ubiquitously employed in high power laser technology, amplified spontaneous emission (ASE) commonly irradiates a target nanoseconds prior to an ultrashort pulse arrival [1]. This fraction of instantaneous intensity relative to that of the main pulse is known as the intensity contrast level. If the contrast level is not sufficiently high the laser will initiate a preplasma expansion [2], altering the initial conditions upon which highly nonlinear ultrashort laser plasma interactions have been shown to sensitively depend, such as in ion acceleration [3–5] or harmonic generation [6]. Debate continues over the optimum level of ASE for different experiments but consensus exists in that it should be known and controlled in order to advance the interpretation of experimental laser plasma physics.

Amongst an array of methods for enhancing the intrinsic laser contrast [7], the plasma mirror (PM) [8] is one which can be incorporated into the experimental set up to further increase the on target contrast by more than two orders of magnitude. Employing a PM results in a considerable reduction in the energy delivered to target, typically in the region of 15–30% per PM interaction and consequently a reduction in interaction intensity. This large energy loss can make the PM an unattractive solution when investigating interaction physics which sensitively depend on intensity or energy scaling, particularly where multiple PMs are used. However, this article will present results showing that large energy loss may be effectively mitigated.

Many high power laser plasma experiments have employed PMs to date, with some studies being dedicated to understanding the characteristics of these optical switches [8–10]. Under certain conditions, the post PM interaction laser far field has been measured to be of good quality [10] and the time resolved reflectivity has also been measured up to ten picoseconds after a femtosecond interaction [11]. An ellipsoidal, focussing PM configuration has also been shown, in principle, to be a capable replacement of the final focussing optic in the laser system [12]. However, there have been no direct measurements of the duration for which the PM surface retains its high optical quality. This usable time window measurement is of particular interest in the context of

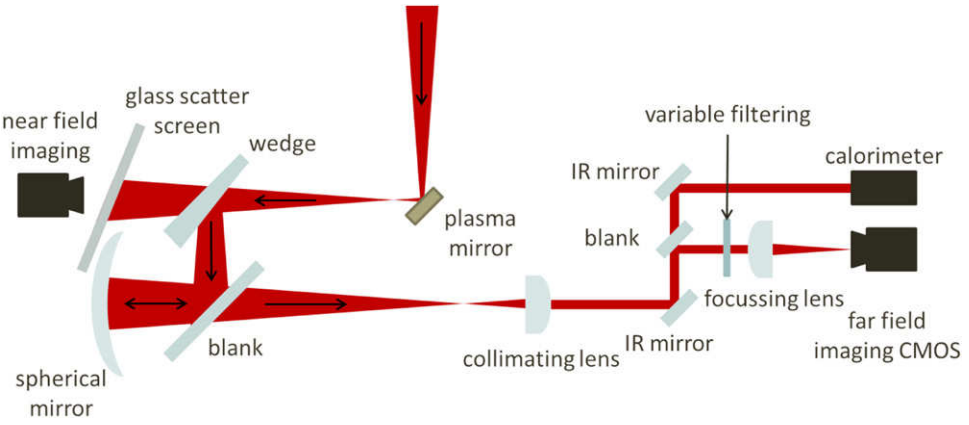

Figure 1. Schematic of experimental set up detailing the positions of infrared glass blanks and wedges used for energy mitigation and imaging optics.

establishing the applicability of PMs in experiments utilizing double pulsing techniques, which have been shown to notably enhance the conversion efficiency of laser energy into protons [13–16] and to provide an optical means of hot electron divergence control [17–19]. With multiple laser pulses also being shown to be more efficient at plasma channelling [20–22], double pulsing could conceivably be of use in relativistically induced transparency based ion acceleration mechanisms, in which the initial target plasma conditions are necessarily controlled through high contrast interactions [23, 24].

In this work, two pulses with a variable temporal delay interact with a PM surface. First, a controlled prepulse is introduced to ionize the PM and then by measuring the far field and specularly reflected energy fraction of the more intense, reflected main pulse, the optimum working conditions of the PM are identified.

2. Experimental method

The experiment was carried out using the PHELIX laser [25] at the GSI facility, the contrast of which has been extensively characterized by Wagner *et al* [26]. A schematic of the experimental set up is given in figure 1, where a 12 cm apertured beam is focussed in an $f/12.5$ cone, in s-polarization relative to the PM surface. The PM is a BK7 glass substrate with a SiO_2 and ZrO_2 double layer coating, designed to minimize reflectivity to less than 0.25% for the 1054 nm laser wavelength at the 45°angle of incidence. The PM therefore potentially offers a factor of up to four hundred in contrast enhancement.

The PM was positioned 2.5 mm from focus, giving an elliptical spot measuring $200 \times 200\sqrt{2}$ μm on the PM surface and a maximum intensity greater than 10^{15} W cm^{-2} could be reached using the 1 J deliverable by the preamplifiers of the laser system.

After the PM interaction, energy needs to be dumped before the far field can be imaged without damaging the CMOS detector. An uncoated wedge and series of infrared glass blanks transmit the majority of the energy, while the weaker, relatively B-integral free, reflected beam is retained for imaging. This is done via a spherical mirror, which subtends an $f/5.3$ collection angle to ensure effective light collection and an achromatic lens, which delivers the beam to two diagnostic branches.

On the first branch, a magnifying telescope arrangement, filtered for 1054 nm, is used to image the far field on an 8 bit CMOS detector, while a Gentec pyroelectric power meter allows absolute calorimetry of the beam on the second branch, the measurement uncertainty of which the manufacturer quotes as being ±2.5% at 95% confidence level. With the rise time of the calorimeter being on the hundreds of microsecond range, multiple pulses arriving on a picosecond time frame will not give a measurably different temporal response between single and double pulse operation for the same total energy. As the CMOS dynamic range is limited, variable optically reflective filtering was installed on this line, such that when the laser energy was varied, a good signal to noise far field image was obtained. The maximum accumulated B-integral on this imaging line was calculated as 5×10^{-2}, based on the nonlinear refractive index of BK7 glass [27], which is considered to introduce negligible distortion.

Near field imaging on the glass scatter screen shown in figure 1 allowed the light collection of the spherical mirror to be calculated as >99% of the reflected beam in all cases [28]. In addition to the on shot set up, an equivalent plane monitor (not shown) acted as a far field reference against the relatively more complex post PM imaging line.

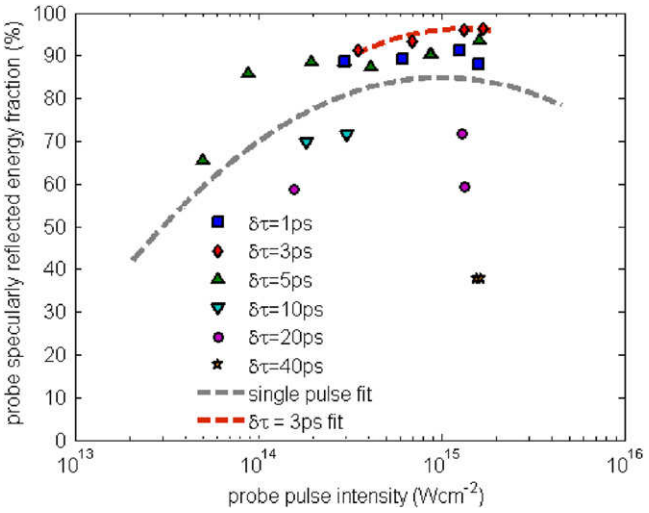

Figure 2. The intensity dependent plasma mirror specular reflectivity curves for the main pulse alone, measured at various time delays relative to the prepulse. A fit to the data of the single pulse case is shown for reference and a fit of the same form is shown for the 3 ps delay scan to guide the eye. The experimental data was obtained here for a prepulse to main pulse intensity ratio of 1:8.

Prior to preamplification, the laser pulse was passed through a Mach–Zehnder style split recombination system in the laser front end. A half waveplate initially rotates the polarization and in this way the relative energy of the pulses can be controlled by using a polarizing beam splitter. The lower energy prepulse later has its polarization corrected by a second half waveplate to match that of the main pulse. With the prepulse taking a fixed path through the system, the relative timing of the beams is controlled by sending the high energy main pulse through a variable delay line. This setup also preserves the 500 fs full width at half maximum duration of both pulses.

The inter pulse time delay was characterized using a single shot autocorrelator. At a nominal 4 ps delay, the maximum error associated with the delay time was ±500 fs, corresponding to an inter pulse time delay error of ±12.5%.

3. Experimental results and modelling

Prior to double pulse testing, the PM operation in the single pulse mode was extensively characterized and the intensity dependent specular reflectivity curve was obtained [28], this is represented by a fit in place of individual data points in figure 2 to preserve the clarity of the plot. A peak reflected energy fraction of 86% was observed at an intensity of 10^{15} W cm^{-2}, for a single pulse interaction.

The behaviour of the PM was investigated with a prepulse:main pulse intensity ratio set at 1:8, for time delays in the range of 1–40 ps. Here, the temporal dependence of the reflected energy fraction and far field intensity distribution of the main pulse are discussed in turn. The trends are described via numerical and analytic modelling of the plasma conditions set up by the prepulse, which are in effect the initial conditions encountered by the main pulse.

3.1. Variation of the specularly reflected energy fraction with time delay-experimental results

When the intensity ratio of the pulses are known, the specularly reflected energy fraction of the prepulse can be calculated from the single pulse reflectivity curve. This allows the single time integrated calorimetry measurement of the total specularly reflected energy to be deconvolved into its component prepulse and main pulse contributions. Using this, the specularly reflected energy fraction of the main pulse alone was calculated over a range of time delays and intensities and is shown in figure 2. This shows two clear trends. Firstly, the low intensity reflected energy fraction of the main pulse has a different intensity dependence when compared to that for a single pulse; secondly there is a strong dependence of the reflected energy fraction on time delay.

In the case of a single pulse, the increasing reflectivity with incident intensity from $10^{13}-10^{15}$ W cm^{-2} is predominantly associated with the leading edge of the pulse ionizing the PM at earlier time. In the double pulse case, however, once the PM is ionized by the prepulse, the main pulse encounters preformed, over critical expanding plasma. This effect is clearly observed for a 10^{14} W cm^{-2} main pulse intensity in the 5 ps delay scan, where the reflected energy fraction is well in excess of that measured for a single pulse. The relatively small enhancement of the main pulse reflectivity at 5×10^{13} W cm^{-2}, is consistent with the prepulse approaching the

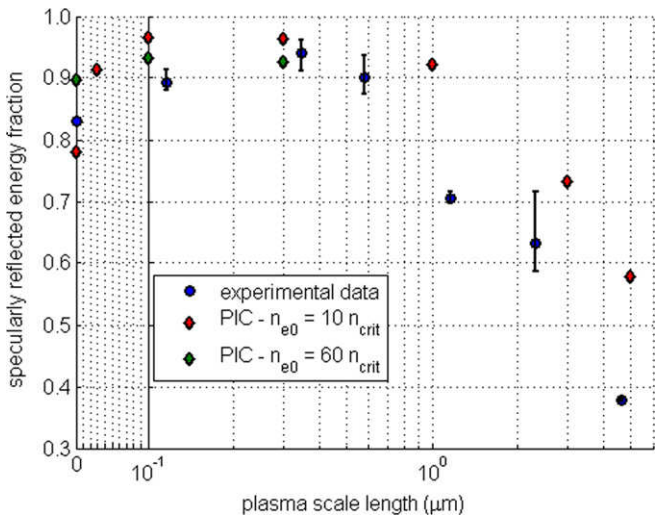

Figure 3. The scale length dependence of the main pulse reflected energy fraction. Error bars represent the range of the experimental measurement over the $2 \times (10^{14} - 10^{15})$ W cm^{-2} intensity range. In order to include the single pulse reflectivity measurements at a scale length of 0 μm, the x-axis is presented on a linear scale for short scale lengths and logarithmic scale for long scale length. This is compared with the modelled reflected energy fraction from 1D collisional PIC simulations described in the main body of the text.

ionization threshold of the PM at the 1:8 intensity ratio. The small enhancement observed here is consistent with spatial variations in the near field intensity profile leading to only the most intense region of the prepulse creating overdense plasma.

Figure 2 clearly shows a considerable enhancement in main pulse reflectivity for pulse separation times of up to 5 ps. A maximum main pulse specularly reflected energy fraction of 96% was determined at a time delay of 3 ps, by deconvolving the double pulse measurement, compared to the 86% measured for a single pulse interaction.

The specularly reflected energy fraction averaged over the $2 \times (10^{14} - 10^{15})$ W cm^{-2} intensity range is given in figure 3 and error bars show the range in reflectivity over this intensity range. Here, the time delay has been transformed to the plasma scale length that the main pulse encounters as a consequence of the prepulse interaction, as per the discussion to follow.

The observation of the peak specularly reflected energy at a temporal delay of 3 ps is intriguing as it implies that the increasing reflected energy fraction must arise from some inherent property of the evolving plasma itself. Understanding this aspect of the plasma which leads to the enhanced reflectivity is key to harnessing the potential to achieve increased PM reflectivity in the future. One of the most obvious differences in the plasma conditions encountered by the main pulse is the evolving plasma density scale length as the plasma expands after the initial prepulse interaction.

3.2. Variation of the specularly reflected energy fraction with time delay—numerical modelling

To estimate how this plasma evolves over time, the PM surface contaminant layer is assumed to undergo a quasi-neutral self similar plasma expansion of the form given by *Kruer* [29], as in equation (1), where $c_s = \sqrt{Zk_B T_e/m_i}$, is the ion sound speed.

$$n_e(x, t) = Zn_i(x, t) = n_{e0} \exp\left(-\frac{x}{c_s t}\right). \quad (1)$$

With the laser radiation pressure estimated to be almost two orders of magnitude lower than the final thermal pressure of the plasma, it is assumed the plasma retains a monoexponentially decaying density profile of the form $\partial n_e/\partial x = n_{e0}/l_{ss}$, characterized by the plasma density scale length, l_{ss}.

The evolving plasma scale length will be determined by the high charge to mass ratio surface contaminant protons, which are consistently observed to be the dominant ion species in laser driven ion acceleration experiments from solid targets [30]. From this, each time delay between the pulses can be expressed in terms of the estimated plasma scale length encountered by the main pulse, as shown on figure 3, which has been scaled by a factor of $\cos^{-1}\theta_i$ to account for the laser angle of incidence. The remaining free parameter is electron temperature seeded by the prepulse, which is estimated as 70 eV from Gibbon's expression [31] of the collisional skin heating model by Rozmus and Tikhonchuk [32] for the prepulse interaction.

One dimensional, collisional particle in cell (PIC) modelling was carried out using the EPOCH code [33], which models collisions based on the Sentoku and Kemp routine [34], to investigate the effect of plasma scale

lengths in the range of 0–5 μm, on laser absorption. A 0 μm scale length represents a single pulse interaction with an initially unperturbed surface and the increasing scale length represents the conditions encountered by the main pulse for increasing time delays.

The unperturbed electron number density, n_{e0}, of the hydrogen plasma is estimated to be in the range of $(1-6) \times 10^{22}$ cm^{-3}. This maximum value is consistent with the number density of protons found in water, while the lower limit reflects that the low temperature 70 eV plasma may be partially ionized and/or have a lower average density than that associated with water.

A 10^{15} W cm^{-2}, 1054 nm main pulse interacts with these plasma conditions, where the spatial resolution was 0.25 nm with a minimum of 30 particles per cell to ensure good statistics and the minimum density was limited to 10^{18} cm^{-3} to relax computation requirements. After reflection from and leaving the plasma region of the simulation box, the energy of the pulse was calculated, allowing the reflected energy fraction to be devised. This is shown next to the experimental data in figure 3.

At such a resolution, running a numerical simulation over the full pulse duration becomes a computationally intensive task and so a 35 fs, full width at half maximum, pulse was used. This therefore gives a scale length dependent reflected energy fraction which is quasi free from the temporal dynamics of plasma expansion during the main pulse interaction. For the assumed preplasma conditions, the plasma expansion in experiment will result in a scale length change of 65 nm over the time that 99% of the energy of the 500 fs, full width at half maximum, Gaussian pulse interacts with the plasma. The average plasma scale length offset for the experimental results is therefore ~33 nm, which soon becomes a negligible contribution to the total scale length.

Qualitatively, good agreement is obtained between the experimental data and numerical modelling trends. For a pulse interacting with an, $n_{e0} = 10^{22}$ cm^{-3}, plasma with steep boundary, representing the case of the single pulse interaction, a reflectivity of 78% is modelled, agreeing well with the 83% average, experimentally measured. A maximum reflectivity of 97% is also found in the PIC modelling for scale lengths less than 1 μm, in extremely good agreement with the 96% measured experimentally and for similar scale length to that assumed by the simple self similar expansion estimate for the experimental data. Where the laser interacts with scale lengths longer than 0.3 μm, PIC modelling predicts that absorption begins to increase as experimentally observed.

In the case of an, $n_{e0} = 6 \times 10^{22}$ cm^{-3} plasma, a similar but less well pronounced trend is observed in the reflected energy fraction. Here, the case corresponding to a single pulse has a relatively high reflectivity of 90% and peaks at 93% for plasma scale lengths of 0.3 μm. For scale lengths of 1 μm and greater the reflected energy fraction matches that of the lower density, $n_{e0} = 10^{22}$ cm^{-3} plasma.

The physical interpretation of this trend in absorption is consistent with the following analysis of the PIC modelling. In the case of an initial step like plasma vacuum boundary, as is most relevant to the conditions of a single pulse interaction, the laser is reflected from high density plasma, where the laser electric field tunnels through the high density barrier with its magnitude being exponentially attenuated. With the electron ion collision time being inversely proportional to the electron density, the excited electrons collide with ions more frequently than in underdense or critical density plasma and the laser energy is efficiently coupled to the high density plasma, leading to a significant absorption fraction.

In the intermediate case of sub micron density scale lengths, the laser is reflected from the lower density critical surface. Although the skin depth of the electric field is longer, it is attenuated in a region of lower density plasma than in the step profile case. This results in exciting electrons in a region of lower electron ion collision frequency and a less efficient transfer of laser energy to the plasma. The plasma reflectivity is therefore increased compared to the short scale lengths.

As the density scale length of the plasma increases further, a more conventional regime of collisional heating takes place, where longer scale length, higher density plasma on the underdense side of the interaction contributes to efficient collisional laser energy absorption.

When n_{e0} is increased from 10^{22} cm^{-3} to 6×10^{22} cm^{-3}, the skin depth, scaling as the inverse of the electron plasma frequency, is reduced, leading to less efficient energy coupling. This is observed for scale lengths shorter than a micron, where the electric field tunnels to regions of higher density plasma. However, for scale lengths of a micron or greater, the density profile in the interaction region is effectively independent of n_{e0}, owing to the critical surface being far away from the unperturbed electron density and the assumed monoexponentially decaying electron number density profile. This leads to the two simulations giving similar reflected energy fractions in long scale length plasma. This general trend is in good agreement with that of Kieffer *et al* [35] for absorption in short scale length plasmas.

The experimentally measured reflected energy fraction at 10 ps delay in figure 3 appears to be in poor agreement with the modelled PM reflectivity, however, this might be due to the reflectivity being experimentally measured at a lower average intensity, where the reflected energy fraction is generally found to be lower.

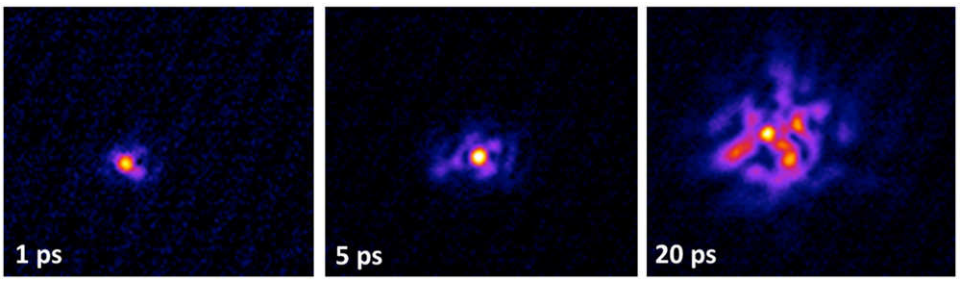

Figure 4. The on shot far field intensity distribution obtained on the prepulse–main pulse shot configuration, for selected time delays as indicated on the bottom left hand side of each image. The experimental data was obtained here for a prepulse to main pulse intensity ratio of 1:8.

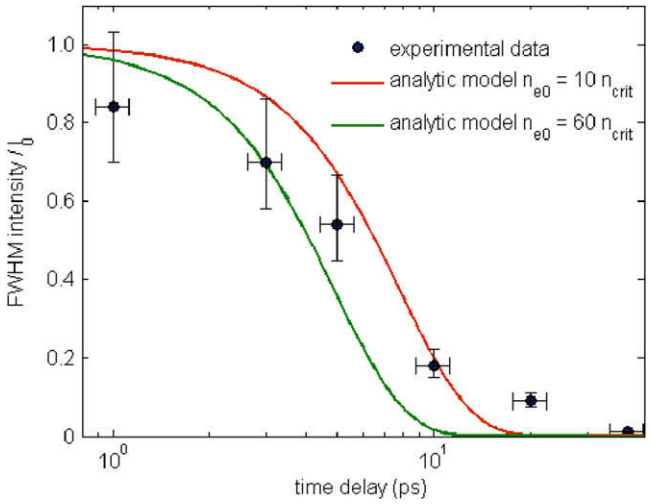

Figure 5. A comparison of the analytical model coherent specular reflected intensity fraction and the experimentally determined equivalent intensity reduction from the effective spot size increase, as discussed in the text. The experimental data was obtained here for a prepulse to main pulse intensity ratio of 1:8.

3.3. Variation of the post PM far field with time delay—experimental results

The on shot far field intensity distributions were also recorded as a function of inter pulse time delay and some examples are shown in figure 4. A clear general deterioration in the far field quality with the PM ionization time was observed and a radial integration technique was used to characterize the extent of this deterioration. From the radial integrals, an *effective spot size* was defined by finding the radius at which half the energy is enclosed. This allows an *equivalent intensity* to be defined, which is proportional to the inverse of the area of the effective spot size. The equivalent intensity therefore does not include information about any intensity increase due to enhanced reflectivity and is intended as a guide only to far field quality, to preserve the simplicity of the model.

The reduction in equivalent intensity is represented on figure 5, where this is normalized to that found for a single pulse interaction. Here, the uncertainty in the half energy spot radius was estimated by testing the reproducibility of the method on nominally similar single pulse intensity distributions.

For time delays of up to 3 ps the far field spot size remains within the uncertainty of that measured for a single pulse, but as time delays increase, more energy is reflected into the wings of the spot and consequently the effective spot size increases. As the delay increases to 10 ps, the increased focal spot sizes results in an order of magnitude in equivalent intensity reduction and for time delays beyond this it is reduced to a few percent of the optimum equivalent intensity.

3.4. Variation of the post PM far field with time delay—analytic model

The distortion of the wavefront at the PM surface is determined by the introduction of phase shifts, $\delta\varphi$, by nonuniform critical surface expansion in the quasi near field of the beam. The maximum phase shift introduced to two rays incident at an angle, θ_i, on a surface with a height perturbation, δx, is given by equation (2).

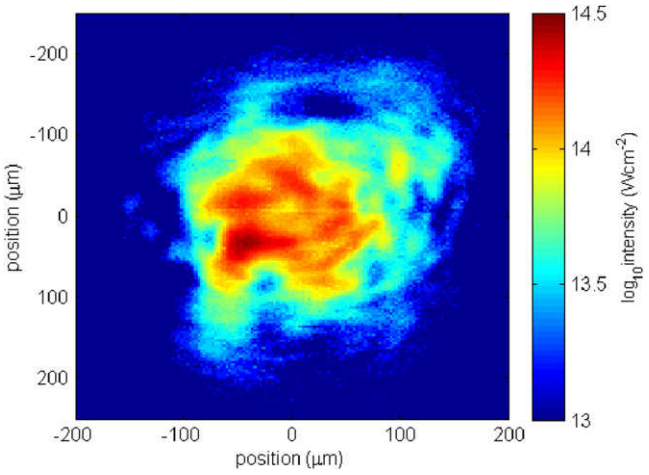

Figure 6. The spatial intensity distribution of the quasi near field incident on the plasma mirror as viewed from a 0° degree angle of incidence.

$$\delta\varphi = \frac{2\pi}{\lambda} 2\delta x \cos\theta_i. \tag{2}$$

A phase shift of zero corresponds to a perfectly smooth surface, while a phase shift of π causes complete destructive interference of the rays. This leads to a $\pi/2$ phase shift being the arbitrary choice in perturbation height, which separates a rough surface from a smooth one, known as the Rayleigh criterion [36].

A statistical treatment of electromagnetic waves incident on a normally distributed surface by Beckmann and Spizzichino [37] yields a similar factor in describing the attenuation of the coherent specularly reflected intensity $\boldsymbol{I}_{\rm coh}$, given in equation (3).

$$\boldsymbol{I}_{\rm coh} = \boldsymbol{I}_0 \exp\left[-\left(\frac{2\pi}{\lambda} 2\sigma_x \cos\theta_i\right)^2 \right]. \tag{3}$$

This eliminates the need for an arbitrary choice of phase shift to separate smooth and rough surfaces by allowing the coherent reflected intensity to be calculated. When the Rayleigh criterion is satisfied, $\boldsymbol{I}_{\rm coh} \approx 0.54\boldsymbol{I}_0$. Here the surface is characterized by a standard deviation of the perturbation height, σ_x, which is assumed to vary slowly compared to the wavelength of the incident radiation.

From equation (1), it can be shown that the critical surface position, $x_{\rm crit}$ [5], from a plasma undergoing a self similar expansion is given by equation (4). As the laser is incident at an angle, this is at a position of lower density than the critical density and the factor, $n_{\rm crit}\cos^2\theta_i$, takes account of this. This allows the difference in the critical surface position, $\mathrm{d}x_{\rm crit}$, to be calculated based on the temperature difference of two points of temperature T_{e1} and T_{e2}, by including the terms in square brackets of equation (4). The critical surface position distribution, characterized by the term $\mathrm{d}x_{\rm crit}$ can then be directly related to the coherent specularly reflected intensity of equation (3).

$$[\mathrm{d}]x_{\rm crit} = \left(\frac{Z}{m_i}\right)^{\frac{1}{2}} \left(k_B^{\frac{1}{2}} T_{e2}^{\frac{1}{2}} \left[-k_B^{\frac{1}{2}} T_{e1}^{\frac{1}{2}}\right]\right) \ln\left(\frac{n_{e0}}{n_{\rm crit}\cos^2\theta_i}\right) t. \tag{4}$$

Using the experimentally measured near field intensity distribution at the PM surface shown in figure 6, an electron temperature was assigned to each point on the PM surface, again from the scaling expressed by Gibbon [31] and based on an average incident intensity at the PM surface of 10^{14} W cm^{-2}. The position of the critical surface with time at each point on the PM surface was calculated using equation (4) for two electron number densities of $(1-6) \times 10^{22}$ cm^{-3} as described earlier.

As the most intense regions of the interaction, which seed a higher electron temperature and faster expansion, will have more influence of the final far field, the temperature is convolved with the laser intensity at each point to weight the contribution to the far field. This convolution is shown in figure 7. This temperature distribution can be transformed into a critical surface position distribution by use of equation (4), the full width at half maximum of which can be related to the perturbation height, σ_x in equation (3), allowing the coherent

[5] On a point of terminology, we define the critical surface as that where reflection takes place, this therefore occurs at a position of reduced density for increasing incidence angle.

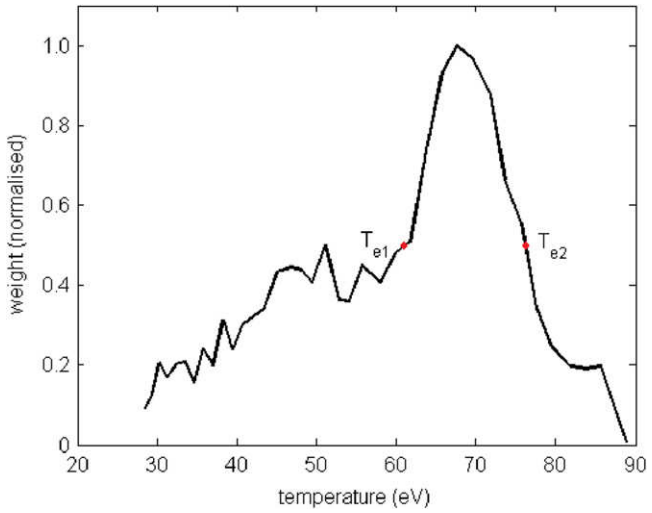

Figure 7. The temperature distribution seeded by the measured spatial intensity distribution incident on the plasma mirror surface. Each temperature is weighted by the incident laser intensity at that point to correlate the position with its influence on the final far field. The temperatures T_{e1} and T_{e2}, as defined in equation (5) are also shown.

specularly reflected intensity fraction to be obtained for various time delays. As the analytical model assumes the characteristic critical surface perturbation size to be normally distributed, this can only be approximated by relating some aspect of the critical surface position distribution, which takes a form qualitatively similar to the temperature distribution of figure 7, to that of a normal distribution and for this reason the full width at half maximum is chosen.

Crucially, the critical surface as a whole can move many times that of the Rayleigh criterion, but it is the temperature differences seeded by the laser that results in expansion velocity differences which themselves cause the critical surface to become more greatly perturbed with increasing time.

The trend of the coherent specular reflected intensity fraction of the analytic model, in figure 5 is qualitatively similar to the equivalent intensity deduced from experimental measurement. Once again, the assumed range in unperturbed electron number density gives good agreement with the experimental data. The higher number density appears to overestimate the degradation time, with the lower limit appearing to underestimate this. At long time delay, both predict a lower intensity fraction than that experimentally measured. This may be a result of assuming a constant expansion velocity, where in reality the plasma expansion will decelerate over time. A slower late time expansion would go some way to explaining why in experiment a more gradual deterioration in the beam quality is observed.

A simple PM temporal window for useful operation, τ_{PM}, which is defined as the time up to which the far field full width at half maximum encircled energy is half of the optimum, can be found from combining equations (3) and (4). Assuming an unperturbed electron density of 10^{22} cm^{-3}, as appears to better fit the experimental data, this condition can be expressed in the convenient form of equation (5), where T_{e1} and T_{e2} are the upper and lower limits of the FWHM of the distribution, as shown in figure 7.

$$\tau_{\mathrm{PM}} < \frac{4.7\ \mathrm{ps}}{T_{e2}^{\frac{1}{2}}(\mathrm{eV}) - T_{e1}^{\frac{1}{2}}(\mathrm{eV})}. \tag{5}$$

With the analytic model assuming a planar one dimensional expansion, this condition is valid when the critical surface displacement is small compared with its gradients across the PM surface. This approach is therefore valid for a smoothly varying intensity profile in this respect.

4. Conclusions and discussion

A main pulse maximum specularly reflected energy fraction of 96 ±2.5% has been experimentally measured, which is the highest reported in the literature to date. This peak PM reflectivity was measured for a inter pulse time delay of 3 ps and numerical modelling via 1D collisional PIC simulations provides good evidence that this is due to the main pulse interaction with evolving plasma density scale lengths.

The best agreement comes from PIC modelling which assumes an unperturbed electron number density of 10^{22} cm^{-3}, where the maximum reflectivity of the PM approaches 97% for scale length around a few tenths of a micron and the single pulse reflectivity agrees to within a few percent. Using this assumption, the general trend

in reflectivity is reproduced well over the scale length range of interest. An assumed unperturbed electron number density of 6×10^{22} cm^{-3}, also reproduces the key trends in reflected energy fraction although less prominently, with a reduced maximum reflectivity and over estimation of the single pulse reflectivity. The unperturbed number density is a parameter that cannot easily be experimentally measured, however the estimated range here provides good agreement with experiment.

Two key predictions are made by the modelling here. These are that control of the density scale length is key to maximizing the specularly reflected energy fraction and that the density scale lengths are dominated by the hydrogen plasma expansion. If the hydrogen layer on the PM surface can be removed by heating [38] or ablation, the plasma density scale lengths might be more readily controlled with their slower expansions dominated by heavier ions. This would have the effect of allowing the maximum reflectivity of the PM to be extended to longer pulse time delays.

The observation of a scale length dependent reflected energy fraction allows us to comment on the likely effect of pulse duration on the reflected energy fraction. Experimental results show that a reflected energy fraction in excess of 90% can be expected for inter pulse time delays of 1–5 ps, or for plasma scale lengths of 0.1–1.0 μm from numerical simulations. This indicates that pulses with duration of 4–7 ps might be expected to exhibit an enhanced reflectivity of around 90% on introducing a similar prepulse to that here. By reducing the main pulse length to 500 fs, it interacts with a plasma scale length that evolves much less over the pulse duration, giving an interaction with a more constrained scale length range for optimal reflectivity. As the pulse duration is decreased further still to 35 fs, the pulse interacts with a quasi constant scale length, which can give a reflected energy fraction of 97%. However, as experimental results show, the 96 ±2.5% reflected energy fraction measured for a 500 fs pulse marks the transition to a pulse duration for which the theoretical maximum reflected energy fraction can be achieved through optimizing the plasma scale length and limiting the extent to which it changes over the pulse duration.

The plasma density scale lengths in the modelling not only reproduce the PM reflectivity curves, but the same self similar expansion and its temporal scaling are also effectively used to reproduce the second key result of this article, the reflected beam quality. The first results reported in the literature are presented here on how the evolving PM surface quality effects the post interaction far field. It has been shown that on this system the PM remains of high optical quality up to 3 ps after ionization with a 1:8 intensity ratio prepulse.

The analytical model shows that nonuniformities in plasma expansion are inextricably linked to the incident laser intensity profile. The nonuniformities in plasma expansion provide an insight into the evolution of the critical surface position, which is used as a basis for relating the critical surface distribution to the coherent specularly reflected energy fraction. The model simplicity is appealing as it gives an estimate of the final far field quality based on only one free parameter, the critical surface roughness, while the other variables, wavelength and angle of incidence are well known. The model yields good agreement with experimental measurements, for the same unperturbed electron number density range as was found to best describe PM reflectivity.

The correlation with the incident PM intensity profile demonstrates that to maintain the far field quality for long time delays, the PM illumination should be kept as uniform as possible. As well as this, the condition given in equation (5) shows the PM usable time window can be extended by using a lower intensity prepulse, seeding a lower temperature plasma expansion with the same intensity distribution. However it should also be noted that the spatial filtering effect of the PM at intensities close to the ionization threshold can lead to the far field becoming reduced in quality when the spatial filtering effectively increases the f-number of the system.

The technique for maximizing the PM reflectivity was achieved here through delivering collinear pulses to the PM surface, however its applicability may be extended for more general use by driving the plasma expansion with a noncollinear pulse to deliver an on target single pulse interaction, while minimizing nanosecond contrast. Alternatively the collinear set up can be kept in experiments where some degree of controlled prepulse is advantageous, as has been demonstrated as highly desirable in double pulse experiments.

Acknowledgments

The authors gratefully acknowledge the expert assistance of the PHELIX operations team. We also gratefully acknowledge funding from EPSRC grant numbers EP/J003832/1, EP/K022415/1 and EP/L001357/1 and from Laserlab-Europe grant no. 284464. The EPOCH code was developed as part of the UK EPSRC funded projects EP/G054940/1. We thank STFC SCARF, on which the numerical simulations were ran. Data associated with research published in this paper can be accessed by contacting the corresponding author.

References

[1] Ivanonv V V, Maksimchuk A and Morou G 2003 Amplified spontaneous emission in a Ti:sapphire regenerative amplifier *Appl. Opt.* **42** 7231
[2] Wagner F *et al* 2014 Pre-plasma formation in experiments using petawatt lasers *Opt. Express* **22** 29505
[3] Neely D *et al* 2006 Enhanced proton beams from ultrathin targets driven by high contrast laser pulses *Appl. Phys. Lett.* **89** 021502
[4] McKenna P *et al* 2006 High-intensity laser-driven proton acceleration: influence of pulse contrast *Phil. Trans. R. Soc.* A **364** 711
[5] Green J S *et al* 2014 Enhanced proton beam collimation in the ultra-intense short pulse regime *Plasma Phys. Control. Fusion* **56** 084001
[6] Zepf M *et al* 1998 Role of the plasma scale length in the harmonic generation from solid targets *Phys. Rev.* E **58** R5253
[7] Danson C, Neely D and Hillier D 2014 Pulse fidelity in ultra-high-power (petawatt class) laser systems *High Power Laser Sci. Eng.* **2** e34
[8] Ziener Ch *et al* 2003 Specular reflectivity of plasma mirrors as a function of intensity, pulse duration, and angle of incidence *J. Appl. Phys.* **93** 768
[9] Doumy G *et al* 2004 Complete characterization of a plasma mirror for the production of high-contrast ultraintense laser pulses *Phys. Rev.* E **69** 026402
[10] Dromey B, Foster P, Kar S and Zepf M 2004 The plasma mirror. A subpicosecond optical switch for ultrahigh power lasers *Rev. Sci. Instrum.* **75** 645
[11] Nomura Y *et al* 2007 Time-resolved reflectivity measurements on a plasma mirror with few-cycle laser pulses *New J. Phys.* **9** 9
[12] Nakatsutsumi M *et al* 2010 Fast focusing of short-pulse lasers by innovative plasma optics toward extreme intensity *Opt. Lett.* **35** 2314
[13] Robinson A P L, Neely D, McKenna P and Evans R G 2007 Spectral control in proton acceleration with multiple laser pulses *Plasma Phys. Control. Fusion* **49** 373
[14] Markey K *et al* 2010 Spectral enhancement in the double pulse regime of laser proton acceleration *Phys. Rev. Lett.* **105** 195008
[15] Scott G G *et al* 2012 Multi-pulse enhanced laser ion acceleration using plasma half cavity targets *Appl. Phys. Lett.* **101** 024101
[16] Brenner C M *et al* 2014 High energy conversion efficiency in laser-proton acceleration by controlling laser-energy deposition onto thin foil targets *Appl. Phys. Lett.* **104** 081123
[17] Robinson A P L, Sherlock M and Norreys P A 2008 Artificial collimation of fast-electron beams with two laser pulses *Phys. Rev. Lett.* **100** 025002
[18] Norreys P A *et al* 2009 Recent fast electron energy transport experiments relevant to fast ignition inertial fusion *Nucl. Fusion* **49** 104023
[19] Scott R H H *et al* 2012 Controlling fast-electron-beam divergence using two laser pulses *Phys. Rev. Lett.* **109** 015001
[20] McKenna P *et al* 2008 Effects of front surface plasma expansion on proton acceleration in ultraintense laser irradiation of foil targets *Laser Part. Beams* **26** 591
[21] Yu W *et al* 2009 Plasma channeling by multiple short-pulse lasers *Laser Part. Beams* **27** 109
[22] Gray R J *et al* 2014 Laser pulse propagation and enhanced energy coupling to fast electrons in dense plasma gradients *New J. Phys.* **16** 113075
[23] Yin L, Albright B J, Hegelich B M and Fernández J C 2006 GeV laser ion acceleration from ultrathin targets: the laser break-out afterburner *Laser Part. Beams* **24** 291
[24] Henig A *et al* 2009 Enhanced laser-driven ion acceleration in the relativistic transparency regime *Phys. Rev. Lett.* **103** 045002
[25] Bagnoud V *et al* 2010 Commissioning and early experiments of the PHELIX facility *Appl. Phys.* B **100** 137
[26] Wagner F *et al* 2014 Temporal contrast control at the PHELIX petawatt laser facility by means of tunable sub-picosecond optical parametric amplification *Appl. Phys.* B **116** 429
[27] Lu X *et al* 2012 Measurement of nonlinear refractive index coefficient using emission spectrum of filament induced by gigawatt-femtosecond pulse in BK7 glass *Appl. Opt.* **51** 2045
[28] Scott G G 2014 On the use of multiple high intensity laser pulses in ion acceleration experiments *PhD Thesis* University of Strathclyde
[29] Kruer W L 1988 *The Physics of Laser Plasma Interactions* (Reading, MA: Addison-Wesley)
[30] Daido H, Nishiuchi M and Pirozhkov A 2012 Review of laser-driven ion sources and their applications *Rep. Prog. Phys.* **75** 056401
[31] Gibbon P 2005 Short pulse laser interactions with matter: an introduction (London: Imperial College Press)
[32] Rozmus W and Tikhonchuk V T 1990 Skin effect and interaction of short laser pulses with dense plasma *Phys. Rev.* A **42** 7401
[33] Brady C S and Arber T D 2011 An ion acceleration mechanism in laser illuminated targets with internal electron density structure *Plasma Phys. Control. Fusion* **53** 015001
[34] Sentoku Y and Kemp A J 2008 Numerical methods for particle simulations at extreme densities and temperatures: weighted particles, relativistic collisions and reduced currents *J. Comput. Phys.* **227** 6846
[35] Kieffer J *et al* 1989 Absorption of ultrashort laser pulse in very steep plasma density gradients *J. Quantum Electron.* **25** 2639
[36] Rayleigh J W S 1897 The theory of sound (Cambridge: Cambridge University Press)
[37] Beckmann P and Spizzichino A 1963 Scattering of electromagnetic radiation from rough surfaces (New York: Macmillan)
[38] McKenna P *et al* 2007 Low- and medium-mass ion acceleration driven by petawatt laser plasma interactions *Plasma Phys. Control. Fusion* **49** B223